Strength of Transverse Fillet Welded Joints

Analysis yields a design formula that is more rational than the method of treating all fillets as though loaded in the weakest direction

BY BEN KATO AND KOJI MORITA

SUMMARY. The resultant force on a fillet weld may be transverse to the axis of the weld, inclined to the axis or parallel to the axis. The stress distribution in the weld and its static resistance vary materially with the relative orientation of load and weld axis.

Most of the basic investigations on the static strength and behavior of fillet welds were conducted during 1920's and 1930's (Ref. 1). It has been shown that breaking loads for transversely-loaded fillets were of the order of 40% greater than those for longitudinally-loaded fillets of the same size and length. In this paper the term transverse fillet will be used to describe the former, while longitudinal fillet will be used for the latter.

A few design specifications (e.g., Ref. 2) and design methods take these differences into account, but most do not, treating all fillet welds as though oriented in the weakest direction. The main reasons for neglecting the greater strength of transverse fillet welds are probably an interest in simplifying design and the fact that the performance of a transverse fillet weld is complex.

Recently, in recognition of the remarkable improvement in quality of steel, electrode and welding techniques, extensive investigations on fillet welded joints were conducted to obtain more rational design formulas (Refs. 3, 4).

Regardless of whether or not one distinguishes between the different types of fillet weld loads in design, it is desirable to make a study of their performance. It should aid in assessing the true effectiveness of connections proportioned by conventional methods.

In this report, the static strength and behavior of transverse fillet welds are studied theoretically. An approximate solution based on the theory of elasticity is reviewed and supplemented by an elastic-plastic-strain hardening analysis performed numerically using the finite element technique. The results are compared with available test results.

BEN KATO is Professor and KOJI MORITA is Assistant Professor in the Faculty of Engineering, Department of Architecture, University of Tokyo, Tokyo, Japan.

An Approximate Approach from the Theory of Elasticity

An approximate theory on the strength of transverse fillet welds was presented by a senior writer (Ref. 5), based on the following assumptions::

1. The direct stress (q) on the tensile face of the weld is uniformly distributed (Fig. 1).
2. The pattern of the elastic stress distribution remains unchanged until the breaking of the weld.
3. Breaking will occur when the shear stress at a point of the fillet reaches

$$\tau_{max.} = \sigma_T / \sqrt{3}$$

where σ_T = the tensile strength of the weld metal.

For simplicity, a fillet weld with equal legs is considered.

The elastic stress components in a fillet are expressed in a polar coordinate system with the origin O at the toe of the fillet, as shown in Fig. 1. The compatibility equation is (Ref. 6).

$$\left(\frac{\partial^2}{\partial r^2} + \frac{1}{r}\frac{\partial}{\partial r} + \frac{1}{r^2}\frac{\partial^2}{\partial \theta^2}\right)\left(\frac{\partial^2 \Phi}{\partial r^2} + \frac{1}{r}\frac{\partial \Phi}{\partial r} + \frac{1}{r^2}\frac{\partial^2 \Phi}{\partial \theta^2}\right) = 0 \qquad (1)$$

The general solution for this equation is

$$\begin{aligned}\Phi = {} & a_0 \log r + b_0 r^2 + c_0 r^2 \log r + d_0 r^2\theta + a_0'\theta \\ & + (a_1 r\theta \sin\theta)/2 + (b_1 r^3 + a_1' r^{-1} + b_1' r \log r)\cos\theta \\ & - (c_1 r\theta \cos\theta)/2 + (d_1 r^3 + c_1' r^{-1} + d_1' r \log r)\sin\theta \\ & + \sum_{n=2}^{\infty}(a_n r^n + b_n r^{n+2} + a_n' r^{-n} + b_n' r^{-n+2})\cos n\theta \\ & + \sum_{n=2}^{\infty}(c_n r^n + d_n r^{n+2} + c_n' r^{-n} + d_n' r^{-n+2})\sin n\theta \end{aligned} \qquad (2)$$

Taking into account the boundary conditions, stress components are obtained from Eq. (2) as

$$\sigma_r = \frac{1}{r}\frac{\partial \Phi}{\partial r} + \frac{1}{r^2}\frac{\partial^2 \Phi}{\partial \theta^2} \qquad (3)$$

$$= \frac{q}{1-\pi/4}\left[\sqrt{2}\sin\theta\cos(\theta-\pi/4)+(\theta-\pi/4)\right]$$

$$\sigma_\theta = \frac{\partial^2 \Phi}{\partial r^2} \qquad (4)$$

$$= \frac{-q}{1-\pi/4}\left[\sqrt{2}\cos\theta\sin(\theta-\pi/4)-(\theta-\pi/4)\right]$$

$$\tau_{r\theta} = \frac{1}{r^2}\frac{\partial \Phi}{\partial \theta} - \frac{1}{r}\frac{\partial^2 \Phi}{\partial r\,\partial \theta} \qquad (5)$$

$$= \frac{-q}{1-\pi/4}\left[\sqrt{2}\sin\theta\sin(\theta-\pi/4)\right]$$

The coordinate θ which yields maximum shear $\tau_{\theta,max}$ is obtained as follows:
From Eq. (5),

$$\frac{\partial \tau_{r\theta}}{\partial \theta} = \frac{-\sqrt{2}\,q}{1-\pi/4}\left[\sin\theta\cos(\theta-\pi/4) + \cos\theta\sin(\theta-\pi/4)\right] = 0$$

From which, $\theta = \pi/8$. Introducing $\theta = \pi/8$ into Eq. (5).

$$\tau_{r\theta\,max.} = \sqrt{2}\,q\,(1-\pi/4)^{-1}\sin^2\pi/8$$

The expression in terms of the external load T_t per one fillet weld is

$$\tau_{r\theta\,max.} = (1-\pi/4)^{-1}(\sin^2\pi/8)(T_t/A_w) \qquad (6)$$

The maximum strength of a transverse fillet weld is obtained by introducing
$\tau_{r\theta,max.} = \sigma_T/\sqrt{3}$ in Eq. (6):

$$T_{t\,max.} = (1-\pi/4)(\sin^{-2}\pi/8)\,A_w\,\sigma_T/\sqrt{3} \qquad (7)$$

The oblique plane RP in Fig. 1 which is normal to the coordinate line $\theta = \pi/8$ through the root of the weld can be considered the fracture plane, that is, breaking will occur along the plane RP making the angle $\theta = \pi/8$ with the shear face.

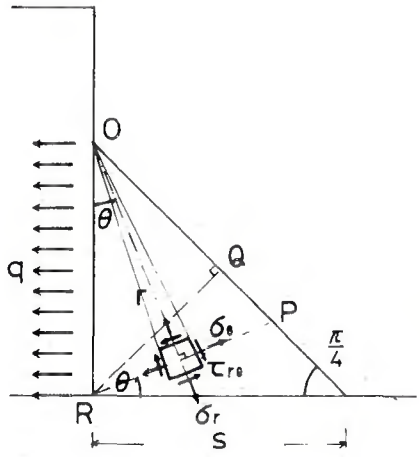

Fig. 1 — Transverse fillet weld

For the case of the longitudinal fillet weld the critical section is clearly the throat (RQ in Fig. 1). Then the maximum strength of a longitudinal fillet weld of the same size and length is

$$T_{l,max.} = A_w\,\sigma_T/\sqrt{3} \qquad (8)$$

From Eqs. (7) and (8),

$$T_{t\,max.} = (1-\pi/4)(\sin^{-2}\pi/8)\,T_{l,max.} = 1.46\,T_{l,max.} \qquad (9)$$

Thus, the present method predicts that transverse fillet welds are 46% stronger than longitudinal fillet welds of the same size and length.

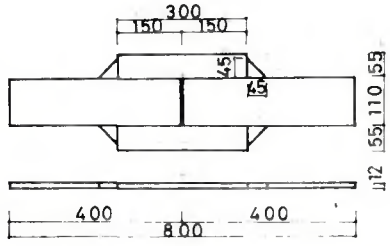

(a) TEST SPECIMENS (in mm.)

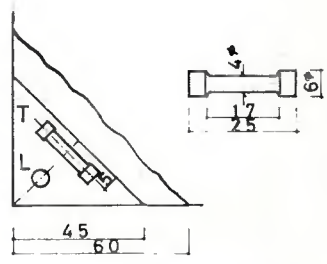

(b) TEST PIECES MILLED OUT OF THE WELD METAL (in mm.)

Fig. 2 — Test specimens (Test No. 1)

Comparison with Test Results

The theoretical prediction obtained in the previous section is now compared with available test results.

One test was performed using specimens of the form shown in Fig. 2(a), where slice-cut specimens with large size fillets were adopted (Ref. 5). Mechanical properties of steel plates and weld metal are shown in Table 1; those of weld metal were obtained from small tensile test pieces machined out of the actual fillets as shown in Fig. 2(b). The experimental maximum strength of joints is compared with the theoretical prediction in Table 2. Figure 3 compares theoretical and test results for the angle the breaking plane makes with the shear face.

Additional tests were performed using specimens of the form shown in Fig. 4, consisting of several sizes of fillets and a limited fillet length (Ref. 7). Mechanical properties of plates and weld metals are shown in Table 3. Test results are compared with the theoretical predictions in Fig. 5 and Table 4. Figure 5 compares the maximum strength while the angle of breaking plane is compared in Table 4. In both cases, the correlation between tests and theory is quite good.

The approximate theory also seems to be able to give a good explanation for the results of group tests cited earlier (Refs. 3, 4). The results of tests carried out by the task committee of AWS Structural Welding Committee shows that for test specimens of A 441 steel welded with E70XX type

Notation

A_w = $l * a$ = throat area
a = $s/\sqrt{2}$ = throat
D^P = elastic-plastic material stiffness matrix
E = Young's modulus
H' = strain hardening modulus
l = length of a fillet
q = uniformly distributed stress on the tensile face of a fillet
s = size of a fillet
T_1 = external load per one longitudinal fillet weld
T_t = external load per one transverse fillet weld
$\Delta\epsilon$ = increment of strain vector
$\Delta\bar{\epsilon}^P$ = equivalent plastic strain increment
ν = Poisson's ratio
$\sigma_r, \sigma_\theta, \sigma_x, \sigma_y$ = normal stress components
σ_x', σ_y' = deviatoric stress
$\bar{\sigma}$ = equivalent stress
σ_T = tensile strength of the weld metal
$\Delta\sigma$ = increment of stress vector
$\tau, \tau_{r\theta}, \tau_{xy}$ = shear stress components
Φ = stress function defined by Eq. (2)

electrodes, the average ratio of the strength of transverse fillet welds to that of longitudinal fillet welds is 1.56 and for specimens of A 514 steel welded with E110X type electrodes, the average ratio is 1.45 (Ref. 3). It has also been found that the results of the international tests conducted under the aegis of the International Institute of Welding, incorporating results from more than ten countries, could be well interpreted on the basis of this theory (Refs. 4, 8).

Analysis by the Finite Element Method

The assumptions made in the derivation of the mentioned solution are not precise. In conjunction with (1), it is known that the direct stress on the tensile face of the weld varies approximately linearly from the toe to the root. As for the assumption (2), the peak stress predicted by elastic theory should be relieved by plastic deformation as soon as it exceeds the yield stress and thus a redistribution of the stress will occur. With respect to the third assumption, the breaking stress should be evaluated according to an appropriate failure theory.

In addition, the shear stress along the assumed breaking plane RP is expressed as

$$\tau = \frac{\sigma_r - \sigma_\theta}{2} \sin 2\beta - \tau_{r\theta} \cos 2\beta$$
$$\beta = 5\pi/8 - \theta \qquad (10)$$

From Eqs. (3), (4), (5) and (10), the distribution of shear stress along the plane RP is given as shown in Fig. 6. This means that $\tau_{r\theta\,max.}$ is not the maximum shear stress along the oblique plane RP. Obviously this result comes mainly from the assumption (1) mentioned above.

In spite of those shortcomings, the prediction from this approximate theory had shown satisfactory agreement with various tests results. More precise study on the performance of the transverse fillet weld in elastic-plastic range is desirable in order to know how this approximate solution can predict the actual behavior and to assert the generality of this solution.

For this purpose, a numerical analysis by the finite element method, extended to the elastic-plastic-strain hardening range by Pope and others (Refs. 9, 10), is applied herein. Analysis is performed on the basis of incremental strain theory and an isotropic and ductile material assumed to obey the von Mises yield condition with Prandtl-Reuss loading function. The principal feature of this problem lies in the evaluation of the elastic-plastic material stiffness matrix D^P which relates the strain increment to the stress increment of the material. D^P is given in Refs. 9, 10, as follows:

$$D^P = \frac{E}{c_2} \quad \text{multiplied by} \qquad (11)$$

$$\begin{bmatrix} \sigma_r'^2 + 2c_1 & -\sigma_x'\sigma_y' + 2\nu c_1 & -\left(\frac{\sigma_x' + \nu\sigma_y'}{1+\nu}\right)\tau_{xy} \\ & \sigma_x'^2 + 2c_1 & -\left(\frac{\sigma_y' + \nu\sigma_x'}{1+\nu}\right)\tau_{xy} \\ \text{(SYM.)} & & c_3 \end{bmatrix}$$

$$\Delta\sigma = D^P \Delta\epsilon, \quad \Delta\sigma = \{\Delta\sigma_x, \Delta\sigma_y, \Delta\tau_{xy}\}$$
$$\Delta\epsilon = \{\Delta\epsilon_x, \Delta\epsilon_y, \Delta\gamma_{xy}\}$$

where,

$$c_1 = \frac{2H'}{9E}\bar{\sigma}^2 + \frac{\tau_{xy}^2}{1+\nu}$$

$$c_2 = \sigma_x'^2 + 2\nu\sigma_x'\sigma_y' + \sigma_y'^2 + 2(1-\nu^2)c_1$$

$$c_3 = \frac{1}{2(1+\nu)}(\sigma_x'^2 + 2\nu\sigma_x'\sigma_y' + \sigma_y'^2) + \frac{2H'}{9E}(1-\nu)\bar{\sigma}^2$$

$$\left.\begin{aligned} \sigma_x' &= (2\sigma_x - \sigma_y)/3 \\ \sigma_y' &= (2\sigma_y - \sigma_x)/3 \end{aligned}\right\} \text{deviatoric stress}$$

E = Young's modulus

ν = Poisson's ratio

$$\bar{\sigma} = \sqrt{\sigma_x^2 + \sigma_y^2 - \sigma_x\sigma_y + 3\tau_{xy}^2}$$

= equivalent stress

$$H' = \Delta\bar{\sigma} / \Delta\bar{\epsilon}^P$$

= strain hardening modulus

$$\Delta\bar{\epsilon}^P = \frac{2\bar{\sigma}}{3c_2}\left[(\sigma_x' + \nu\sigma_y')\Delta\epsilon_x + (\sigma_y' + \nu\sigma_x')\Delta\epsilon_y + (1-\nu)\tau_{xy}\Delta\gamma_{xy}\right]$$

= equivalent plastic strain increment.

The computational procedure of the problem is outlined in the flow chart of Fig. 7. The detailed description of the analytical process for the similar problem is given elsewhere (Ref. 11).

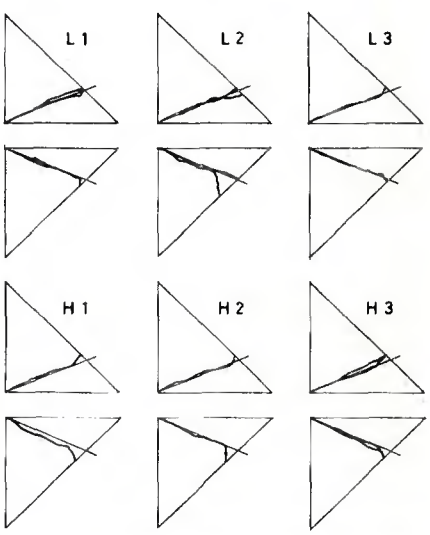

Fig. 3 — Breaking planes, theory and tests

Table 1 — Mechanical Properties of Plate and Weld Metal (Test No. 1)

Property	Steel plate	Weld metal D4316[a] L[b]	D4316[a] T[b]	D4316[a] Mean	D5011[a] L	D5011[a] T	D5011[a] Mean
Yield point (kN/cm²)[c]	27.54	37.73	40.47	39.10	40.67	39.49	40.08
Tensile strength, (kN/cm²)	45.86	47.33	48.22	47.82	51.74	50.27	51.06
Elongation, %	29.0	37.8	28.9	33.4	32.9	33.4	33.2
Reduction of area (%)	—	56.1	45.8	51.0	41.2	39.4	40.3

(a) Type of electrode; D4316: low hydrogen type; D5011: high cellulose type.
(b) L = longitudinal, T = transverse; see Fig. 2(b).
(c) 1 kN/cm² = 1.45 ksi.

Table 2 — Maximum Loads by Tests and Theory (Test No. 1)

	Tests L1	L2	L3	Mean	H1	H2	H3	Mean	Theory L	H
Maximum load, kN	301.84	286.16	319.48	302.82	343.0	311.64	338.1	331.24	307.72	329.28

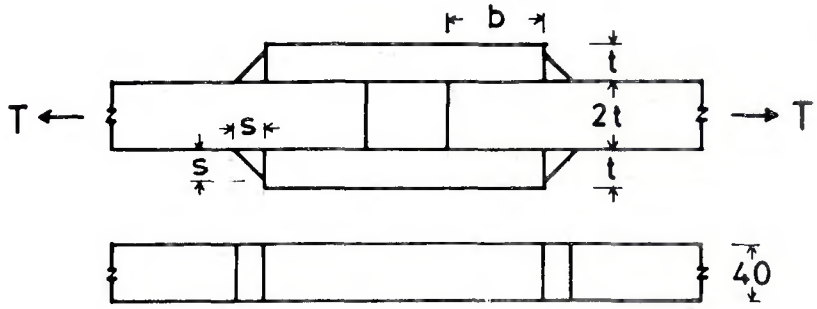

	S5B S5R	S10B	S15B S15R	S20B	S30B	S40B S40R
s	5	10	15	20	30	40
b	27	49.5	72	94.5	139.5	184.5
t	9	16.5	24	31.5	46.5	61.5
B: Basic type electrode, R: Rutile type electrode b=4.5(s+1), t=1.5(s+1), s,b,t, in mm.						

Fig. 4 — Test specimens (Test No. 2)

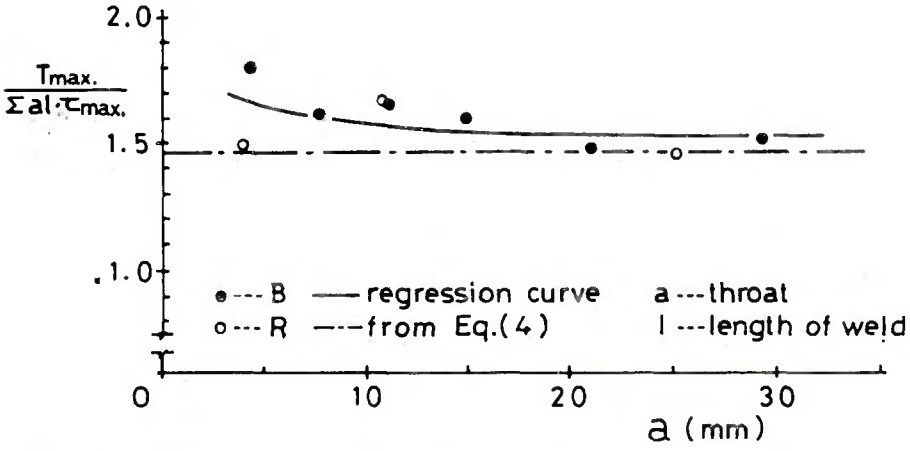

Fig. 5 — Comparison between tests and theory (Test No. 2)

Table 3 — Mechanical Properties of Plates and Weld Metals (Test No. 2)

		Yield point, kN/cm²	Tensile strength, kN/cm²	Elongation, %
Steel plates used with	B-type[a] electrode	33.22	56.25	32.4
	R-type[a] electrode	34.30	55.17	37.4
Weld metals	S5 B	44.88	57.62	21.0
	S10B	44.39	58.80	21.0
	S15B	44.59	58.31	21.7
	S20B	47.04	59.49	19.3
	S30B	47.04	59.49	19.3
	S40B	47.04	59.49	19.3
	S5 R	46.35	56.35	17.5
	S15R	44.59	54.19	18.5
	S40R	45.77	54.59	16.4

(a) B = basic; R = rutile

Table 4 — Angle of Breaking Plane with Shear Face

Specimen	Angle, deg	Specimen	Angle, deg
S5 B	21.0	S20B	22.0
S5 R	20.5	S30B	21.5
S10B	20.5	S40B	21.0
S15B	21.9	S40R	20.5
S15R	21.8	Theory	22.5

The specimen is modeled by triangular elements as shown in Fig. 8. The important results obtained are compared with experimental results and with previous approximate solution in the following.

Elastic Behavior

The distribution of principal stresses in the fillet and its vicinity in the elastic range is shown in Fig. 9. Measured stresses and those calculated by the finite element method are compared in this figure. Measured stresses are obtained from electric resistance wire strain gages installed on the test specimen S40B mentioned earlier (Ref. 12). In the actual specimen, some friction between the inner plate and outer plate is inevitable, while in the analytical model no friction between them is assumed. Considering this difference of condition, the correlation between test and theory seems to be good.

Another comparison of experimental and calculated stresses is given in Fig. 10. The cited test results are taken from Reference B. This test consists of two types of specimen; one has slits along the contact faces of joined plates as seen in Fig. 10(a), the other has joined plates closely in contact as seen in Fig. 10(b). Stresses given in the figure are also those at the load level T=441 kN. Stress measurements were carried out using an extensometer. Principal stresses are shown in the right side of each figure, where mag-

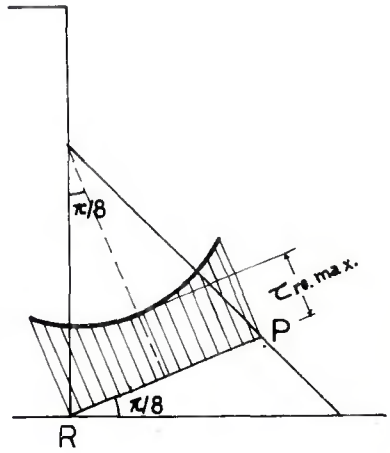

Fig. 6—Shear stress distribution by Eq.(10)

nitudes are given irrespective of their orientation. σ_x , σ_y and τ_{xy} in the left side of each figure are the normal stress component perpendicular to the tensile face, the normal stress component perpendicular to the shear face, and the shear stress along tensile face and shear face, respectively.

In test specimen (b), frictional forces will be induced when the specimen is subject to tension; no friction will appear in specimen (a), but some additional bending due to eccentricity will appear in this case. In the analytical model for the finite element calculation, however, the condition of no gap but no friction between contact faces is assumed, as seen in Fig. 8. The result from the finite element method, Fig. 10(c), shows an intermediate feature between test results of (a) and (b), and taking into account above mentioned situation, the theoretical basis of the finite element computation seems to be reasonable.

Plastic Behavior

Figure 11 shows the spread of the plastic zone for increasing loading steps. When a certain load level (T=849 kN) is exceeded the spread of the yield-flow region expands no further, while the rapid progress of plastic deformation into strain hardening range is observed along a localized area, which approximately coincides with the formerly predicted breaking plane.

Distributions of shear stress along the assumed breaking plane RP are shown in Fig. 12 for various loading steps. Results from the finite element method are given in solid lines. These are different from the pattern given in Fig. 6 the result from the elastic theory, and present no stress peaks at the ends. Rather, they show good agreement up to the ultimate stage with the prediction given by Eq. (6), shown by dashed lines in the figure.

The above observations seem to explain the reason why the approximate solution given by Eq. (7) can provide a satisfactory estimation of the actual strength of the transverse fillet welded joints.

Conclusion

It has been shown that the strength of transverse fillet welded joints could be estimated by Eq. (7) satisfactorily in spite of theoretical shortcomings involved in the basis of its argument. An elastic-plastic analysis by the finite element technique made herein seems to explain the reason why the prediction by Eq. (7) agrees with tests results and thus to support the validity of Eq. (7) from the theoretical side.

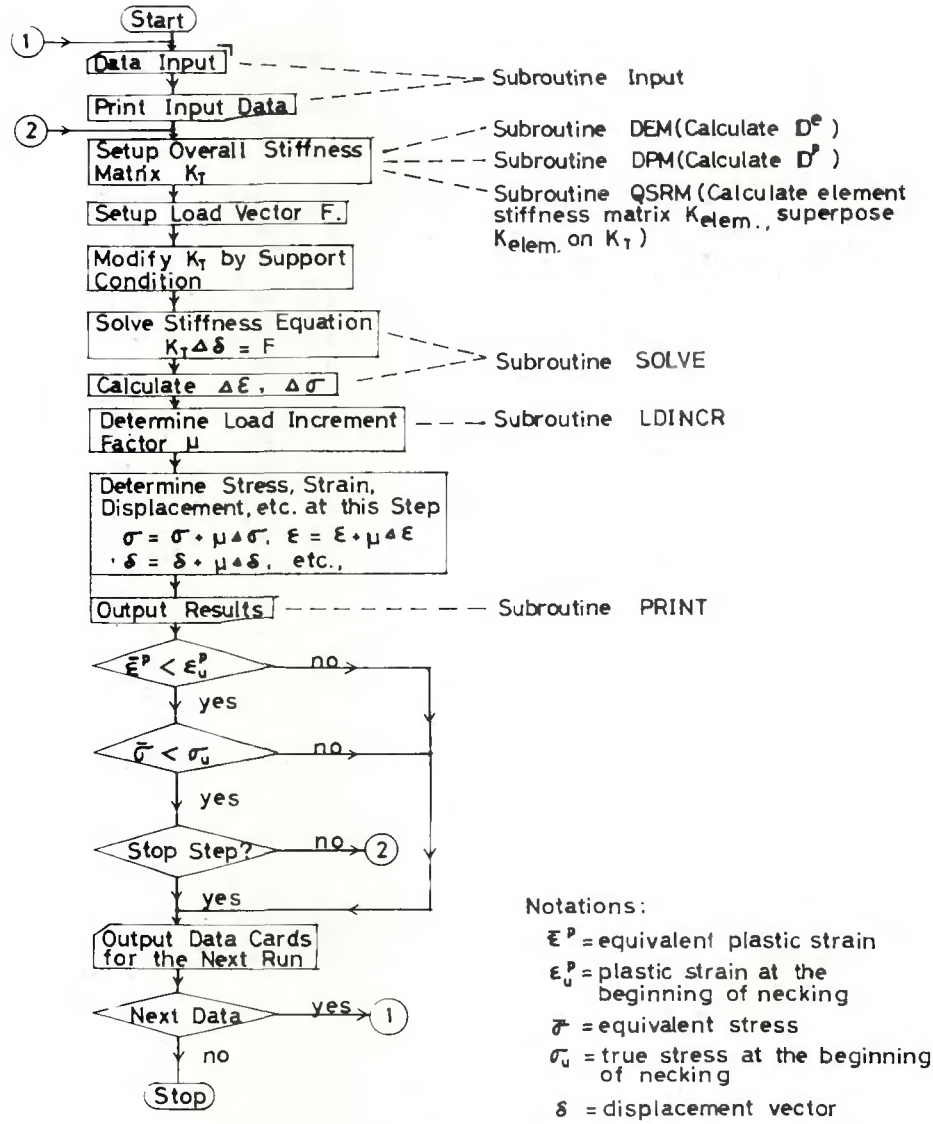

Fig. 7 — Flow chart for computational procedures

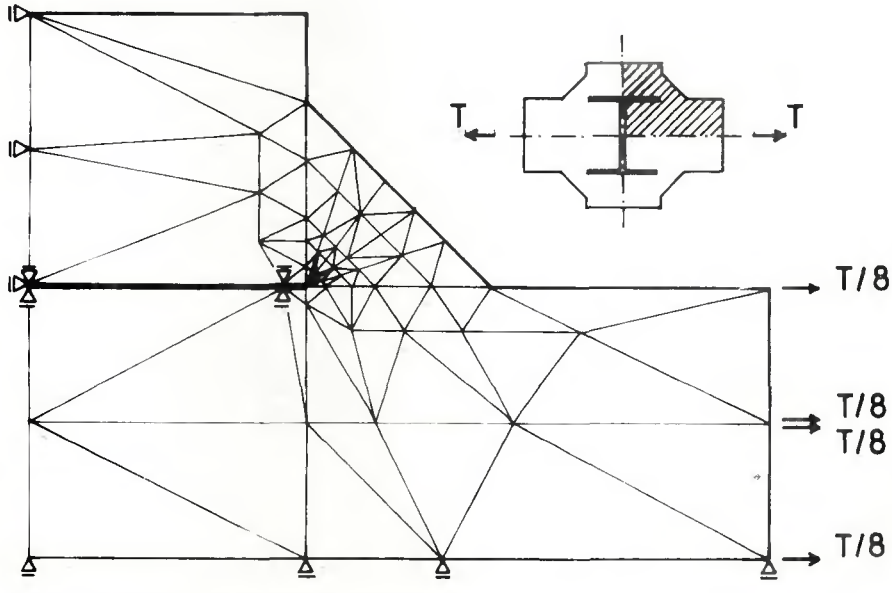

Fig. 8 — Subdivision of the specimen into triangular elements

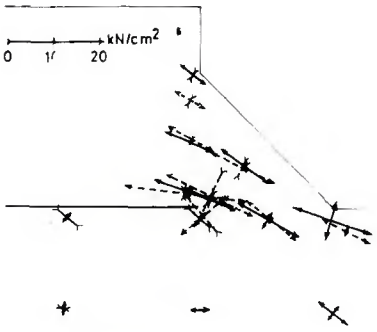

Elastic Range
(T = 441 kN)

← → tension
→ ← compression
—— observed
----- by Finite Element Method

Fig. 9 — Distribution of principal stress

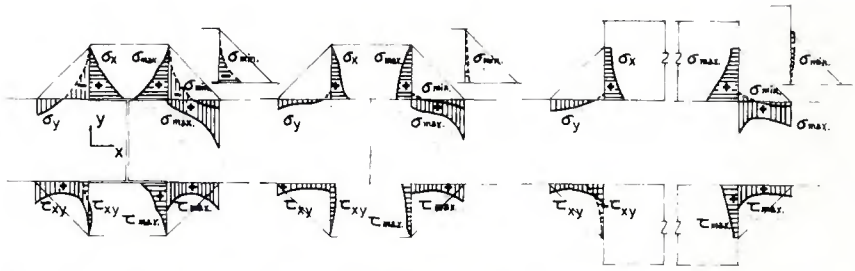

(a) Slits Along Contact Faces (b) Plates Closely Contacted (c) Calculated by Finite Element Method

Fig. 10 — Comparison of stress distributions

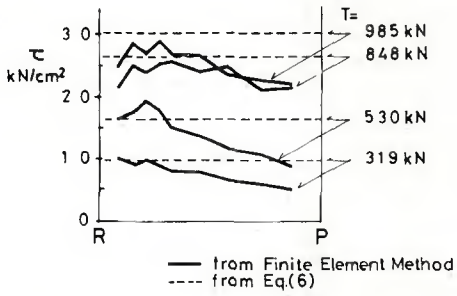

Fig. 12 — Shear stress distribution obtained by finite element method

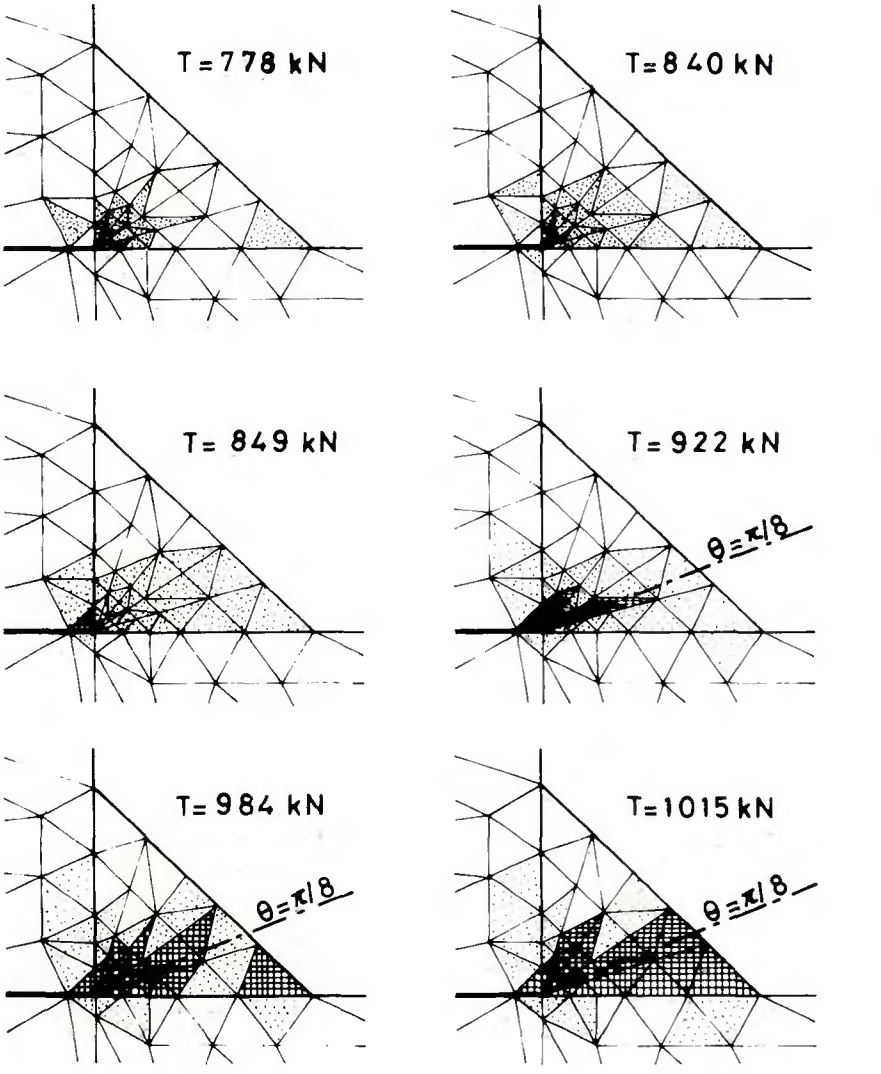

Fig. 11 — Spread of plastic region in a fillet

References

1. Spraragen, W. and Claussen, G. E., Static Tests of Fillet and Plug Welds, a Review of Literature from 1932 to January 1, 1940, *Welding Journal,* April, 1942.

2. American Waterworks Association Standard for Steel Tanks, Standard Pipes, Reservoirs and Elevated Tanks for Water Storage, 1959 ed., (for example).

3. Higgins, T. R. and Preece, F. R., "Proposed Working Stress for Fillet Welds in Building Construction," *Engineering Journal,* AISC, Vol. 6, No. 1, 1969.

4. Ligtenberg, F. K., International Test Series, Final Report, Doc. XV-242-68, I.I.W., 1968.

5. Kato, B. and Naka, T., "Deformation and Strength of End Fillet Welds," *Jour. of the Faculty of Engineering,* University of Tokyo, Vol. XXVIII, No. 3, 1966.

6. Timoshenko, S., *Theory of Elasticity,* McGraw-Hill Book Co.

7. Kato, B., et al., "Ultimate Strength of Fillet Welded Joints," Trans. of Architectural Institute of Japan, Oct. 1968, (in Japanese).

8. Kato, B. and Morita, K., The Strength of Fillet Welded Joints, Doc. XV-267-69, I.I.W., 1969.

9. Pope, G. G., "The Application of the Matrix Displacement Method in Plane Elasto-Plastic Problems," Proc. of the Conference held at Wright-Patterson Air Force Base, Ohio, Oct. 1965.

10. Yamada, Y., et al, "Plastic Stress-Strain Matrix and its Application for the Solution of Elastic-Plastic Problems by the Finite Element Method, *International Journal of Mechanical Sciences,* Vol. 10, No. 5, May, 1968.

11. Kato, B. and Aoki, H., "Deformation Capacity of Steel Plate Elements," Publications of IABSE, Vol. 30-I, Zürich, 1970.

12. Kato, B., et al, "Ultimate Strength of Transverse Fillet Welded Joints," *Trans. of Architectural Institute of Japan,* August, 1969, (in Japanese).

13. Bierett, G. and Grüning, G., "Spannungszustand und Festigkeit von Stirnkehlnahtverbindungen, *Stahlbau,* 10, 1933.

WRC Bulletin
No. 184
June 1973

"Submerged-Arc-Weld Hardness and Cracking in Wet Sulfide Service"

by D. J. Kotecki and D. G. Howden

This study was undertaken to determine:
(1) The causes of higher-than-normal hardness in submerged-arc welds in plain-carbon steels
(2) The levels of strength or hardness which will not be susceptible to sulfide-corrosion cracking
(3) Welding procedures which will assure that nonsusceptible welds will be produced.

Concentration is primarily on weld metal, though some consideration to the weld heat-affected zone is given. The study covered a two-year period. The first year was concerned with a macroscopic view of the weldments. In that first-year study, some inhomogeneities were observed in weldments which are not obvious in a macroscopic view of the weldment. It appeared likely that these inhomogeneities could affect the behavior of the weldment in aqueous hydrogen-sulfide service. Accordingly, their presence and effects were investigated during the second year.

The price of WRC Bulletin 184 is $3.50 per copy. Orders should be sent to the Welding Research Council, 345 East 47th Street, New York, N.Y. 10017.

WRC Bulletin
No. 185
July 1973

"Improved Discontinuity Detection Using Computer-Aided Ultrasonic Pulse-Echo Techniques"

by J. R. Frederick and J. A. Seydel

The purpose of this project, sponsored by the Pressure Vessel Research Committee of the Welding Research Council, was to investigate means for obtaining improved characterization of the size, shape and location of subsurface discontinuities in metals. This objective was met by applying computerized data-processing techniques to the signal obtained in conventional ultrasonic pulse-echo systems. The principal benefits were improved signal-to-noise ratio and resolution.

The price of WRC Bulletin 185 is $3.50 per copy. Orders should be sent to the Welding Research Council, 345 East 47th Street, New York, N.Y. 10017.